Combined emergency braking and turning of articulated heavy vehicles

Graeme Morrison & David Cebon

Published online: 12 Jan 2017.

Submit your article to this journal ⎘

Article views: 238

View related articles ⎘

View Crossmark data ⎘

IA*VSD*

Taylor & Francis
Taylor & Francis Group

🔓 OPEN ACCESS

Combined emergency braking and turning of articulated heavy vehicles

Graeme Morrison and David Cebon

Department of Engineering, University of Cambridge, Cambridge, UK

ABSTRACT

'Slip control' braking has been shown to reduce the emergency stopping distance of an experimental heavy goods vehicle by up to 19%, compared to conventional electronic/anti-lock braking systems (EBS). However, little regard has been given to the impact of slip control braking on the vehicle's directional dynamics. This paper uses validated computer models to show that slip control could severely degrade directional performance during emergency braking. A modified slip control strategy, 'attenuated slip demand' (ASD) control, is proposed in order to rectify this. Results from simulations of vehicle performance are presented for combined braking and cornering manoeuvres with EBS and slip control braking with and without ASD control. The ASD controller enables slip control braking to provide directional performance comparable with conventional EBS while maintaining a substantial stopping distance advantage. The controller is easily tuned to work across a wide range of different operating conditions.

Nomenclature

l_{1f} longitudinal distance from front axle to whole mass CoG on tractor
l_{1r} longitudinal distance from rear axle to whole mass CoG on tractor
l_{2aa} longitudinal semitrailer axle spacing
l_{2r} longitudinal distance from middle axle to whole mass CoG on semitrailer
l_{ic} longitudinal distance from hitch point to whole mass CoG on vehicle unit i
m_i whole mass of vehicle unit i
u_i longitudinal velocity of vehicle unit i
C_α cornering stiffness
I_{izz} whole mass yaw moment of inertia of vehicle unit i
K_r ASD controller gain relating to tractor yaw rate
K_β ASD controller gain relating to tractor side slip
K_γ ASD controller gain relating to articulation angle
β_1 sideslip angle at CoG of tractor unit
δ_{1f} tractor front axle road–wheel steering angle
μ coefficient of friction

CONTACT David Cebon ✉ dc@eng.cam.ac.uk, gm395@cam.ac.uk

ξ slip attenuation factor
$\dot{\psi}_1$ yaw rate of tractor unit
ψ_{12} articulation angle

## Subscripts

$\Box_{1f/1r/2}$ relating to tractor front axle/tractor rear axle/trailer axles
$\Box_{\Box,ref}$ relating to ASD reference model states
$\Box_{\Box,ss}$ steady-state quantity

1. Introduction

Heavy goods vehicles (HGVs) suffer from emergency stopping distances up to 40% longer than those of passenger cars [1]. This is predominantly due to the limited bandwidth of conventional pneumatic electronic/anti-lock braking systems[1] (EBS) for HGVs, causing large amplitude cycling of the wheel state between almost free-rolling and almost fully-locked. Braking forces are therefore sub-optimal for most of the emergency braking event (see Figure 1).

'Slip control' (SC) braking strategies have been proposed for both HGVs and passenger cars [1–11]. SC shortens emergency stopping distances by accurately regulating longitudinal wheel slip to the point of maximum braking force. For HGVs the stopping distance
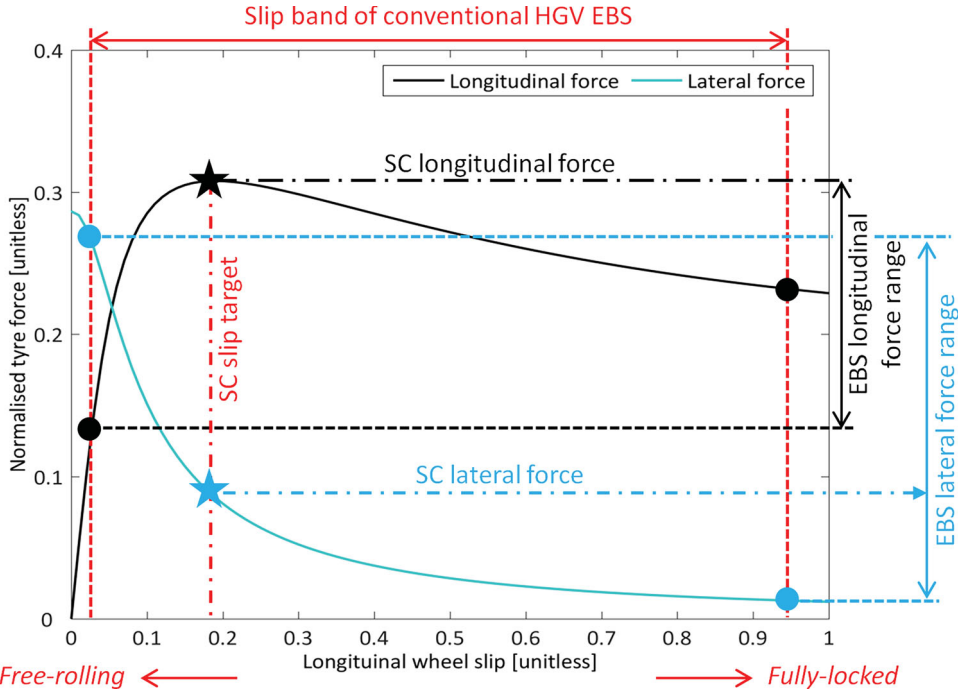
Figure 1. Typical lateral and longitudinal tyre force characteristics against longitudinal slip, plotted using the Fancher tyre model with three degrees sideslip angle and a static friction coefficient of 0.4.

reduction can be substantial. The Cambridge Vehicle Dynamics Consortium (CVDC), for example, demonstrated up to 19% straight-line stopping distance reductions on low friction surfaces, relative to conventional EBS, using a prototype pneumatic SC system on a tractor–semitrailer [11,12].

However, given that the primary function of EBS is to maintain directional stability and controllability during heavy braking [13], there has been surprisingly little research regarding the effects of SC braking on directional performance. According to the tyre force against slip characteristic in Figure 1, when close to free-rolling the tyre can generate large lateral forces but this capacity is substantially reduced as wheel lock is approached. By cycling between these two extremes, a conventional HGV EBS enables large lateral forces to be generated periodically when the longitudinal slip approaches zero. With SC, although the target slip is relatively low, lateral force is significantly reduced for the entirety of emergency braking. The periodic large lateral forces observed with EBS no longer occur. This is likely to impact directional control and stability.

Dincmen et al. [14] simulated a passenger car in combined emergency braking and cornering manoeuvres, with wheel slip controlled to the point of maximum braking force. This caused a substantial reduction of lateral tyre forces and a corresponding degradation of directional vehicle dynamics. An open-loop scheme for 'lateral force improvement' was proposed, targeting a slightly lower level of braking slip during cornering in order to recover lateral forces without significantly increasing stopping distance. Directional performance was improved in a limited range of simulation scenarios; however, the effectiveness of the controller across a broader range of operating conditions or when exposed to disturbances must be questioned due to its open-loop nature.

Kimbrough [15,16] proposed optimal controllers to improve the stability of passenger cars when simultaneously cornering and accelerating/decelerating by only varying longitudinal slip. The controllers were later extended for articulated HGVs [17]. During emergency braking, deceleration would be maximised subject to a stability constraint on the vehicle's yaw dynamics. In order to satisfy the stability constraint, each wheel's longitudinal slip would be reduced as necessary from the value at which maximum braking force would occur. Stability improvements were demonstrated in computer simulations, with up to 10% losses of stopping performance. However, the controllers required numerous states and parameters which are difficult to obtain, including dynamic vertical tyre loads and nonlinear, combined slip tyre characteristics. These issues were never fully addressed and as such the controllers were never implemented on a test vehicle.

This paper begins by presenting a validated nonlinear model of a tractor–semitrailer in Section 2. The model is used in simulations to compare the performance of EBS and SC in combined emergency braking and cornering manoeuvres. Though SC can substantially shorten stopping distances, this is shown to be at the expense of directional performance. In Section 3, an 'attenuated slip demand' (ASD) controller is designed to overcome this. This modified SC strategy aims to restore directional performance to the level of conventional EBS, while maintaining the substantial stopping distance advantage of SC. Simulation results for the ASD controller are presented in Section 4 and tuning is discussed. Section 5 draws conclusions from the paper and outlines plans to conduct vehicle tests using the CVDC's prototype SC system.

2. Simulation model and validation

2.1. Vehicle model

Computer simulations were developed in Simulink based around a nonlinear 16 degrees-of-freedom (DoF) model of a tractor–semitrailer (see Figure 2). When uncoupled, the
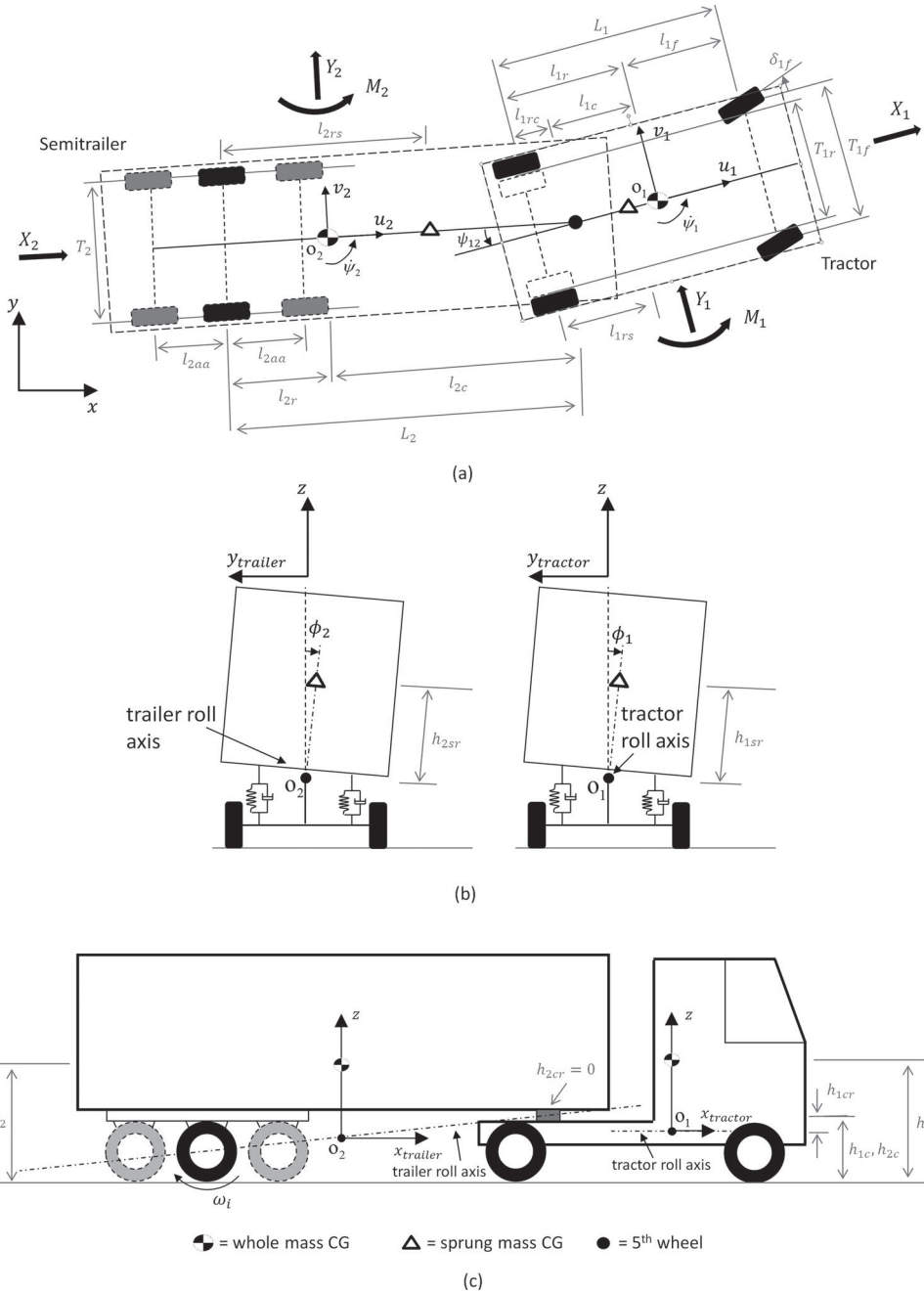

Figure 2. Sixteen DoF nonlinear vehicle model.

rigidly modelled tractor and semitrailer bodies each have four DoFs: longitudinal, lateral, yaw and roll. Kinematic constraints at the hitch point in the longitudinal and lateral directions remove two DoFs, leaving six in total for the vehicle bodies. The rotations of the wheels then provide the additional 10 DoFs. Pitch and bounce of the vehicle bodies and motions of the unsprung axle masses are neglected. The vertical profile of the road surface is modelled as smooth. Longitudinal load transfer is calculated according to the longitudinal accelerations of the vehicle bodies, while lateral load transfer also includes the dynamic effects of body roll. Tyre forces are calculated using Fancher's nonlinear, combined slip truck tyre model [18]. Equations of motion and parameters for the vehicle model are detailed in full in [19].

2.2. Braking system sub-models

Two different braking system sub-models were combined with the vehicle model, representing a conventional EBS and an idealised SC system, respectively.

2.2.1. Conventional EBS

Miller [20] experimentally validated an EBS model for HGVs based on earlier work by Kienhöfer [21]. The model produced brake pressure and wheel speed fluctuations similar in both magnitude and frequency to experimental data for a Haldex EB+ system. Stopping distances on a low friction surface were predicted to within 3% accuracy. The same model is deployed in this paper. Key features include:

- the driver's brake pedal demand modelled as a step input, with a low-pass filter and rate limit applied to remove unrealistically high-frequency content;
- anti-lock braking control logic consisting of five possible states: monitoring, prediction (pressure drop), reselection, fast pressure rise and slow stepping pressure rise;
- transfer functions modelling the EBS modulator valve characteristics;
- a fixed time delay and low-pass filter between the EBS modulator valves and brake chamber pressure, to capture delayed pneumatic response in the air lines and brake chamber.

Further detail regarding the EBS sub-model and its parameters can be found in [19].

2.2.2. Idealised slip control

The idealised SC model assumes that the slip of each wheel is perfectly regulated to the value at which braking force is maximised. This is implemented in the simulation by calculating the required slip values based on the known tyre model, then applying these slips to the vehicle model as inputs. Although this idealised performance could never be completely realised in the presence of disturbances, noise, uncertain parameters and bandwidth limits, it is a reasonable approximation of current high-bandwidth prototype systems. Accurate regulation of slip has been demonstrated in real vehicle tests with the CVDC's prototype system [11,22] and various methods have been proposed by which to estimate the optimum slip value for braking [10,23]. As SC technology continues to improve, the idealised SC model should become an ever more accurate approximation.

2.2.3. Assumptions regarding electronic stability control

EBS systems on state-of-market HGVs are typically (and in most nations required to be) combined with an electronic stability control (ESC) system. ESC augments the yaw stability of the vehicle by applying a corrective yaw moment through differential braking. If the vehicle is already braking maximally, it may achieve this by reducing brake pressure on one side of the vehicle.

In this paper all braking systems have been modelled with the assumption of no ESC functionality, i.e. no ability to deliberately apply a corrective yaw moment by differential modulation of brake pressure between the vehicle's left- and right-hand wheels. This decision was taken because ASD serves the function of anti-lock braking on a state-of-market system, but not ESC. ASD regulates longitudinal wheel slip in order that during emergency braking, sufficient lateral tyre forces can be generated on all axles for the driver to maintain control of the vehicle. It does not directly augment the yaw stability of the vehicle by differential braking to apply a corrective yaw moment. However, such ESC functionality could be integrated with either SC or ASD braking in a similar manner to its integration with anti-lock braking on state-of-market systems. Therefore, the fairest baseline for comparison is the state-of-market EBS with ESC disabled. Future research may investigate the integration of ESC with ASD or SC braking, in which case a comparison against a full EBS/ESC system should be made.
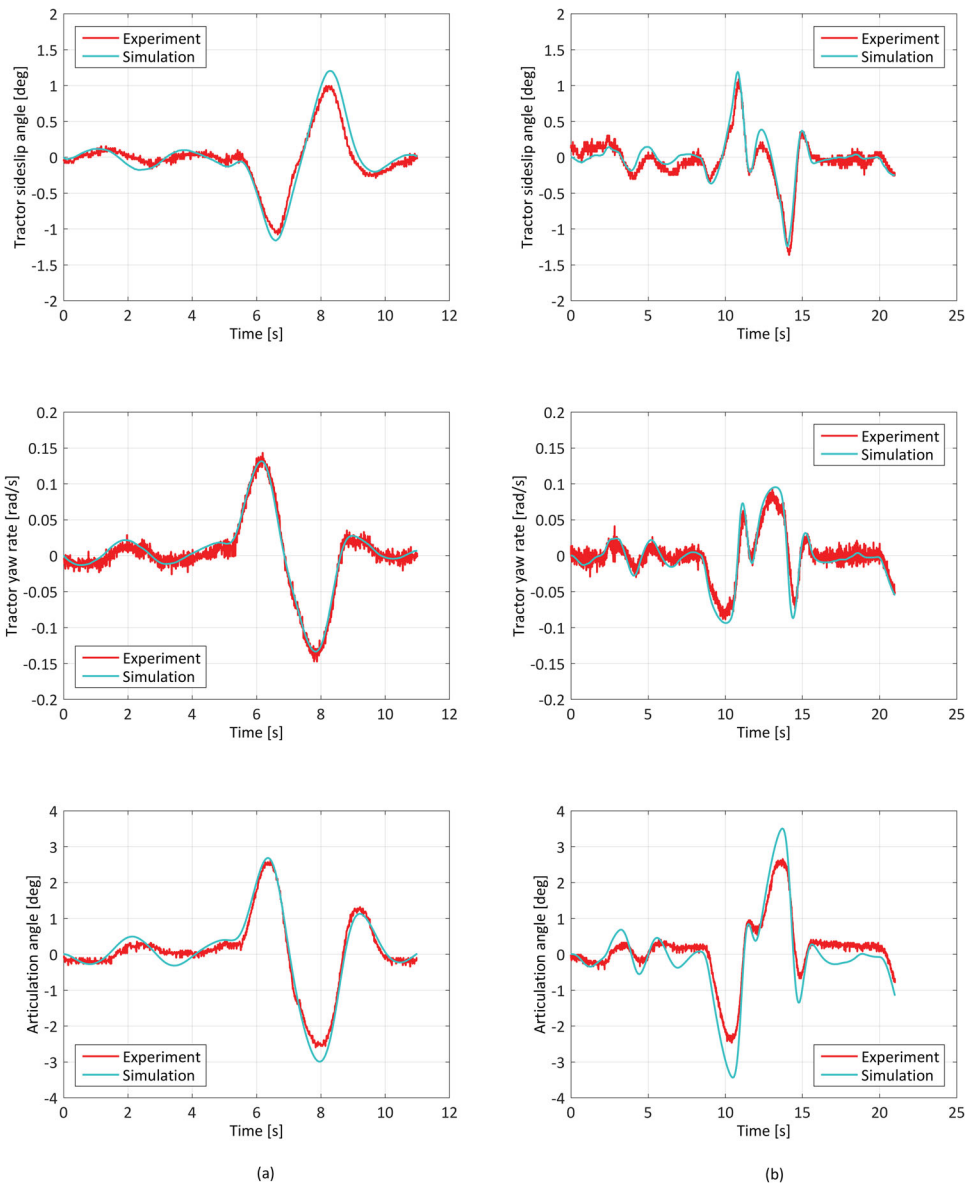
2.3. Validation

The model was experimentally validated using a full-scale tractor–semitrailer. The vehicle's ESC and traction control systems were disabled, but anti-lock braking remained enabled. The tractor unit was fitted with a Knorr-Bremse EBS 5 braking system, which is close to state-of-the-art having only recently been succeeded by the EBS 7 in 2013. The trailer unit was fitted with a Haldex EB+ Generation 1 system, which is somewhat more outdated but would have been state-of-the-art until 2009 when the Haldex EB+ Generation 2 system was introduced.

The tractor unit was instrumented with an RT3022 inertial/GPS navigation system to measure forward velocity, yaw rate and sideslip angle at the centre of gravity (CoG). The trailer was instrumented with a calibrated VSE articulation angle sensor. Additional sensors were also installed to measure wheel speeds and tractor front axle road–wheel steering angle, since data on the J1939 chassis CANbus from the vehicle's existing sensors were only available at a sampling frequency of 10 Hz. Data from the additional instrumentation were sent via CANbus to a computer in the tractor cab running Matlab xPC Target and logged at 100 Hz.

Figure 3 shows a selection of results from the validation of the model's lateral dynamics. Lane change manoeuvres were performed on high ($\mu \approx 0.9$) and low ($\mu \approx 0.1$) friction surfaces. The measured tractor front axle road–wheel steering angle from the experiments was input to the vehicle model in Simulink and the corresponding simulated vehicle responses were overlaid with the test data. The sideslip angle and yaw rate of the tractor unit and articulation angle are shown. Good agreement can be observed between the experimental and simulated results in both manoeuvres.

Figure 4 shows a selection of results from the validation of the model's longitudinal dynamics. Vehicle speed and wheel speed traces are compared between simulation and
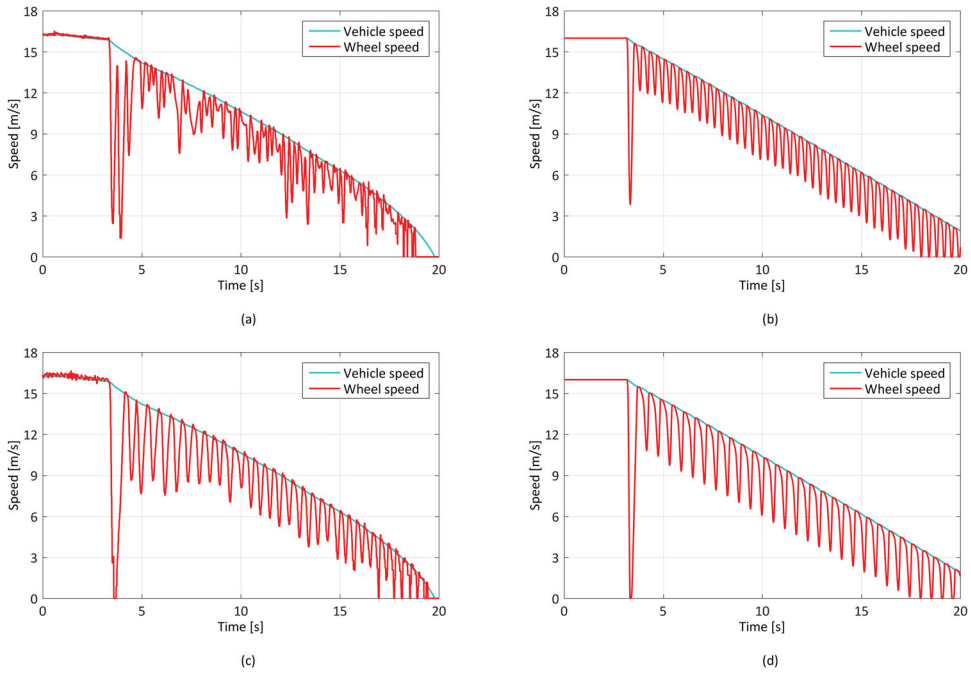
Figure 3. Validation of lateral vehicle dynamics. Comparison of simulation and experiment for (a) high friction ($\mu \approx 0.9$) and (b) low friction ($\mu \approx 0.1$) lane change manoeuvres.

experiment, for the tractor front and trailer middle axles, in a straight-line anti-lock braking event from 60 km/h on the low friction surface ($\mu \approx 0.1$). Good qualitative agreement can be observed in both cases and the magnitude and frequency of the wheel speed cycles are reasonable. Stopping distance was predicted to within 2% accuracy by the model in this manoeuvre.

Only a brief selection of the model validation results has been discussed above. Full details of the experiments and further results and discussion can be found in [19].

Figure 4. Validation of the EBS sub-model and longitudinal vehicle dynamics. Comparison of simulated and experimental vehicle speed and wheel speed traces in an emergency stop from 60 km/h on a low friction surface ($\mu \approx 0.1$): (a) tractor front left wheel – experiment; (b) tractor front left wheel – simulation; (c) trailer middle left wheel – experiment and (d) trailer middle left wheel – simulation.
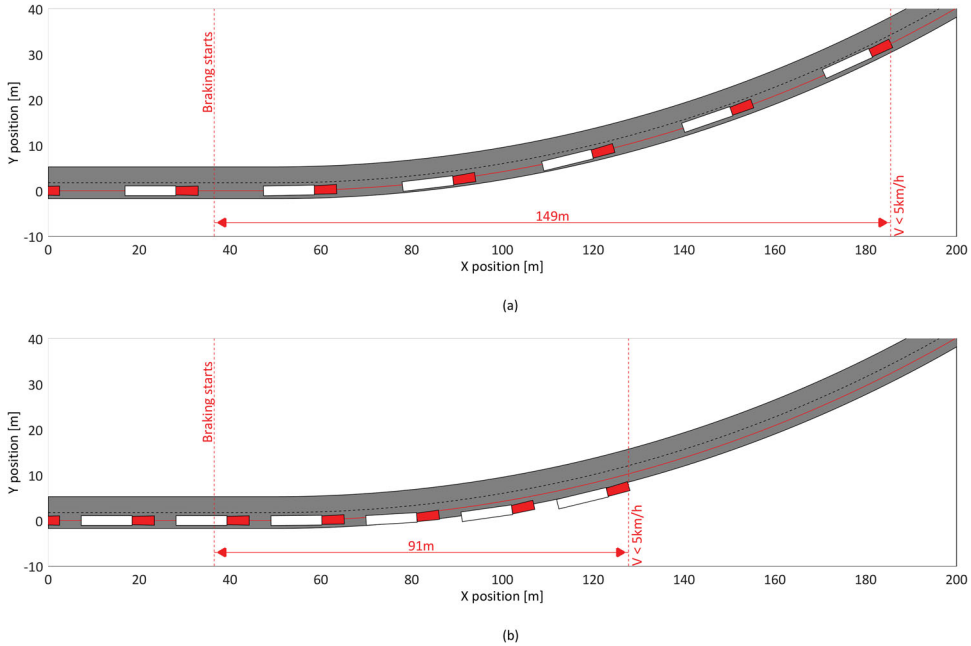
Figure 5. Animations of simulation results for (a) conventional EBS and (b) SC emergency braking in a 300 m radius J-turn manoeuvre.

2.4. Comparison of EBS and slip control

The validated vehicle model was combined with a single preview point closed-loop driver model, which steers to follow a predefined reference path. A preview time of 0.8 s and proportional, integral and derivative gains of 0.04 rad/m, 0.01 rad/(m s) and 0.01 rad s/m, respectively, were used for the driver model. Further description of the driver model can be found in [19]. A 300 m radius J-turn manoeuvre (straight approach followed by a constant radius corner) on a surface with $\mu = 0.4$ was simulated from an initial speed of 88 km/h, with emergency braking commencing when the driver model began to steer into the turn. The simulation ended when the vehicle speed fell below 5 km/h.

Figure 5 compares animations of the vehicle's behaviour with conventional EBS and SC. With EBS, the vehicle had a long stopping distance but was able to remain within a 3.5 m wide road lane for the entire manoeuvre. With SC stopping distance was substantially reduced, but the vehicle understeered severely out of the lane. This provides motivation to research alternative SC braking strategies, aiming to improve directional performance while still maintaining as short a stopping distance as possible.

3. Attenuated slip demand controller

3.1. ASD concept

Figure 6 shows the same lateral and longitudinal tyre force characteristics as in Figure 1. When operating at peak braking force, a small reduction of longitudinal slip causes only a
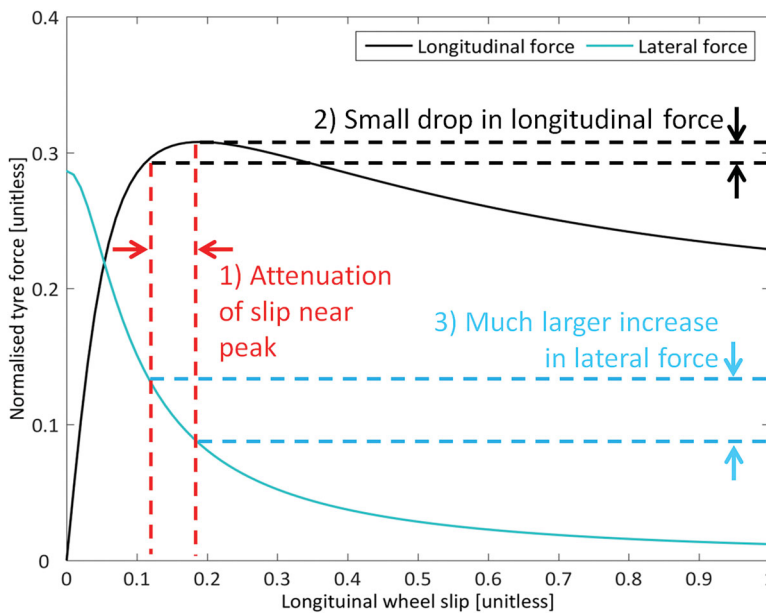
Figure 6. Attenuated slip demand (ASD) concept. A small reduction of longitudinal slip when operating at the peak value provides a significant improvement in lateral tyre force (at a given tyre sideslip angle) for only a small drop in longitudinal force.

small loss of longitudinal force. However, because the gradient of the lateral curve is considerably steeper in the same slip range, this is accompanied by a much larger increase in lateral force. Therefore by demanding slightly attenuated levels of slip with the SC system, it should be possible to substantially improve directional performance with minimal increase in stopping distance. This 'ASD' concept is essentially the same as exploited both by Dincmen et al. [14], Kimbrough [15,16] and Kimbrough et al. [17].

A new closed-loop control strategy to exploit this ASD concept is outlined below. In comparison to the controllers of Kimbrough [15,16] and Kimbrough et al. [17], it should lend itself better to a real-time practical implementation on a HGV in light of the following attributes:

- it is computationally inexpensive, since no online optimisation is required;
- all controller inputs can either be measured or estimated using inexpensive or standard sensors, or are already required for slip control braking;
- no information or assumptions regarding the vehicle's nonlinear, combined slip tyre characteristics are necessary.

3.2. Controller design

Figure 7 is a high-level block diagram of the ASD controller. In keeping with the architecture of the CVDC's prototype HGV slip control system, it is assumed that there is a global controller for the vehicle and a local slip controller at each wheel station. The local controllers receive slip demand signals from the global controller and regulate slip to these levels. The ASD controller operates within the global controller, as a 'bolt-on' to the existing SC system.

The controller incorporates a reference vehicle model (see Section 3.2.1) requiring two inputs: tractor front axle road–wheel steering angle and longitudinal vehicle speed. As a pre-requisite for slip control braking, an accurate estimate of longitudinal vehicle speed is
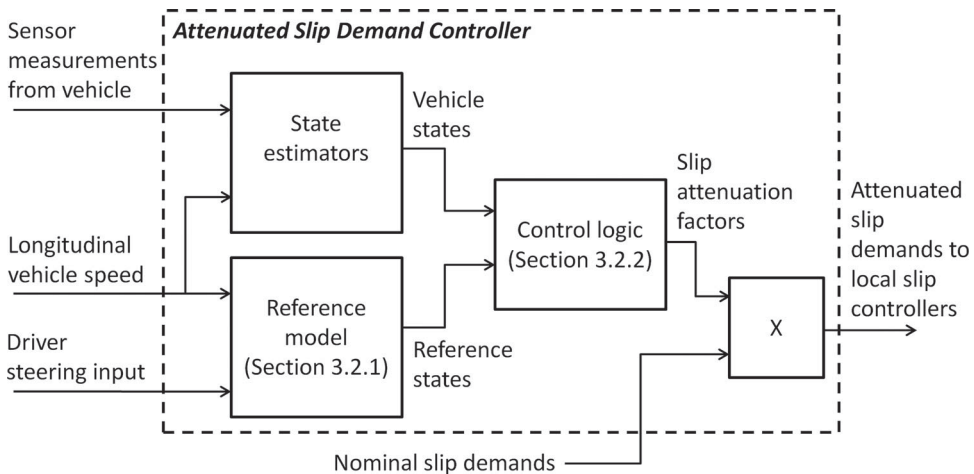
Figure 7. High-level block diagram of proposed ASD controller.

assumed to be available. The reference model outputs a set of reference states to which the actual vehicle states can be compared.

Most of the necessary vehicle states can be directly measured using inexpensive or standard sensors. The exception is sideslip angle of the tractor unit. Morrison and Cebon [24,25] address sideslip angle estimation for a tractor–semitrailer, including when manoeuvring at the limits of tyre adhesion due to low friction or heavy braking. The simulations in this paper assume that accurate and noise-free measurements of all the necessary states are available.

Control actions are based on heuristic comparisons of the observed and reference vehicle states. These calculations are presented in Section 3.2.2. The output is a set of 'slip attenuation factors', between 0 and 1, for each axle of the vehicle. The nominal slip demands, i.e. those previously used by SC to maximise braking force, are scaled by the relevant slip attenuation factors (which are always between 0 and 1). The resulting attenuated slip demands are the final controller outputs, which are sent to the local wheel slip controllers.

3.2.1. Reference model

Figure 8 shows the linear, single-track, yaw-plane reference model of the tractor–semitrailer. The wheels of each axle are replaced by a single effective wheel located on the vehicle's centre-line, with a linear lateral tyre model. Sideslip and articulation angles are assumed small and longitudinal velocity u_1 is constant.

The model can be described in state-space form as

$$\dot{x} = A(u_1)x + B(u_1)\delta_{1f}, \tag{1}$$

where $x = [\beta_1 \ \dot{\psi}_1 \ \dot{\psi}_{12} \ \psi_{12}]^T$ (tractor sideslip angle, tractor yaw rate, articulation rate and articulation angle), δ_{1f} is the tractor front axle road–wheel steering angle and matrices $A(u_1)$ and $B(u_1)$ are given in Appendix 1. For a given steering angle and longitudinal velocity, the steady state can be calculated as

$$x_{ss} = -A(u_1)^{-1}B(u_1)\delta_{1f}, \tag{2}$$

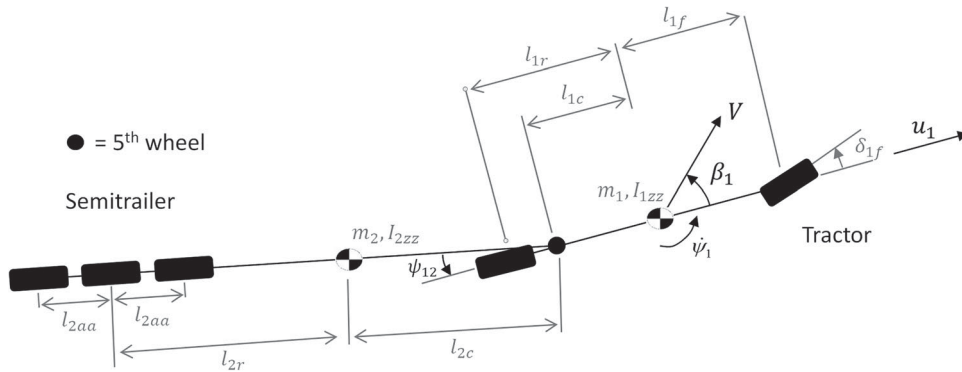**Figure 8.** Single-track yaw plane reference model for ASD controller.

where $x_{ss} = [\beta_{1,ss} \ \dot{\psi}_{1,ss} \ 0 \ \psi_{12,ss}]^{\text{T}}$. This steady-state vector forms the basis of the reference state vector:

$$x_{ref} = \begin{bmatrix} \beta_{1,ref} & \dot{\psi}_{1,ref} & \psi_{12,ref} \end{bmatrix}^{\text{T}} = \begin{bmatrix} 0 & \dot{\psi}_{1,ss} & \psi_{12,ss} \end{bmatrix}^{\text{T}}. \qquad (3)$$

By basing the reference states on the steady-state solution of the model, they are independent of the yaw moments of inertia of both tractor and semitrailer. The only necessary parameters are therefore the tyre cornering stiffnesses, mass and longitudinal CoG position for the tractor and semitrailer, plus geometric information such as wheel spacing and fifth wheel or kingpin location. Geometric properties can be accurately known, since they are easily measured and do not tend to change during service. Also, it is now common for HGV tractors to estimate combination mass and static tractor axle loads online [26] based on air suspension pressures. Therefore if the static axle loads of the uncoupled tractor unit (which should have little variation) are known, both tractor and semitrailer mass and CoG position can be calculated from these estimates. This leaves only tyre cornering stiffness parameters to be determined for the reference model. Other researchers have proposed and successfully tested online methods by which to estimate these parameters for a linear, single-track model of a tractor–semitrailer [27].

Note that a zero tractor sideslip reference was used in Equation (3), instead of the compatible steady-state sideslip. Either is common when designing vehicle dynamics controllers [28–31]. Both approaches were investigated for the ASD controller, with the zero sideslip reference found to give marginally better results.

3.2.2. Control calculations
The time-varying slip attenuation factors ξ_{1f}, ξ_{1r} and ξ_2 for the tractor front, tractor rear and trailer axles are given by the following equations:

$$\xi_{1f} = \max(1 - K_r|\dot{\psi}_1 - \dot{\psi}_{1,ref}|H(|\dot{\psi}_{1,ref}| - |\dot{\psi}_1|) - K_\beta|, \ \beta_1 - \beta_{1,ref}|, 0), \qquad (4)$$

$$\xi_{1r} = \max(1 - K_r|\dot{\psi}_1 - \dot{\psi}_{1,ref}|H(|\dot{\psi}_1| - |\dot{\psi}_{1,ref}|) - K_\beta|\beta_1 - \beta_{1,ref}|, \ 0), \qquad (5)$$

$$\xi_2 = \max(1 - K_\gamma|\psi_{12} + \beta_1 - \psi_{12,ref}|, \ 0), \qquad (6)$$

where $H(x)$ is the Heaviside step function:

$$H(x) = \begin{cases} 0 & \text{if } x \le 0, \\ 1 & \text{if } x > 0, \end{cases} \qquad (7)$$

and K_β, K_r and K_γ are positive gains relating to the tractor sideslip, tractor yaw rate and articulation angle, respectively. These must be tuned. The control actions resulting from Equations (4)–(6) can be described as follows. If the tractor unit understeers, the Heaviside step function in Equation (4) attenuates the slip demand for the tractor front axle to restore its lateral tyre forces. If the tractor unit oversteers, the Heaviside step function in Equation (5) attenuates the slip demand for the tractor rear axle to restore its lateral tyre forces. If the tractor unit sideslips excessively, Equations (4) and (5) together attenuate the slip demands for both tractor axles to restore their lateral tyre forces. Finally if the trailer begins to swing out, Equation (6) attenuates the slip demands for all trailer axles to restore their lateral tyre forces.

It is important to distinguish between two different possible causes of large articulation angle error: trailer swing-out and jack-knife. Trailer swing-out is caused by reduced lateral tyre forces on the trailer, therefore braking on the trailer should be attenuated. By contrast the jack-knife scenario, where the trailer 'pushes' the tractor unit around to a large yaw angle, is caused by reduced lateral tyre forces on the tractor rear axle. Attenuating the braking on the trailer wheels would exacerbate the problem in the jack-knife scenario, causing the trailer to further push the tractor unit around.

In order to reduce the attenuation of trailer braking in the jack-knife scenario, tractor sideslip angle β_1 was included in Equation (6). When approaching jack-knife both articulation angle and tractor sideslip angle should become large, but with opposite sign. Therefore, the effective articulation angle error $|\psi_{12} + \beta_1 - \psi_{12,ref}|$, used in Equation (6), becomes large during trailer swing-out but remains small during jack-knife.

## 4. ASD simulation and tuning

4.1. Optimised performance

Simulations of the 300 m radius J-turn manoeuvre described in Section 2.4 were repeated for slip control with ASD. The same assumptions in modelling the braking system were used as for SC, but with the demanded wheel slips attenuated by the ASD controller.

MATLAB's constrained optimisation solver *fmincon* was used to optimise the three ASD controller gains for this specific manoeuvre, so as to maximise the mean deceleration subject to no part of the vehicle leaving a 3.5 m wide road lane centred about the desired path. The simulation was called repeatedly by *fmincon* with the ASD gains as arguments, to evaluate objective function value (mean deceleration) and state of constraints (lane-keeping) for each trialled set of gains, starting from the point $K_\beta = K_\gamma = 20 \, \text{rad}^{-1}$, $K_r = 20 \, \text{s/rad}$.

Figure 9 shows an animation of the manoeuvre for ASD with the resulting set of optimised gains: $K_\beta = 23.5 \, \text{rad}^{-1}$, $K_r = 34.6 \, \text{s/rad}$ and $K_\gamma = 30.8 \, \text{rad}^{-1}$. The entire vehicle remained within the 3.5 m wide road lane throughout the manoeuvre, but with only a marginally greater stopping distance (93 m) than observed for SC in Figure 5 (91 m), and much shorter than EBS (149 m). Mean deceleration was 58% greater than with EBS and only 1.1% less than with SC.

Figure 10 compares various vehicle states throughout the manoeuvre for EBS, SC and ASD with the optimised gains. Figure 10(a) and (b) highlight the 'best of both worlds'
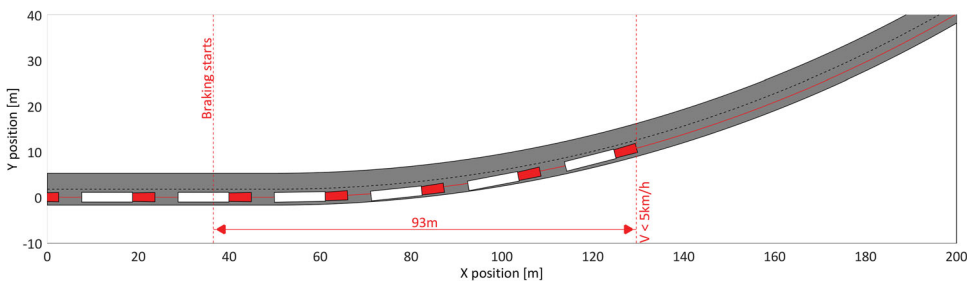
Figure 9. Animation of simulation results for ASD emergency braking in a 300 m radius J-turn manoeuvre.
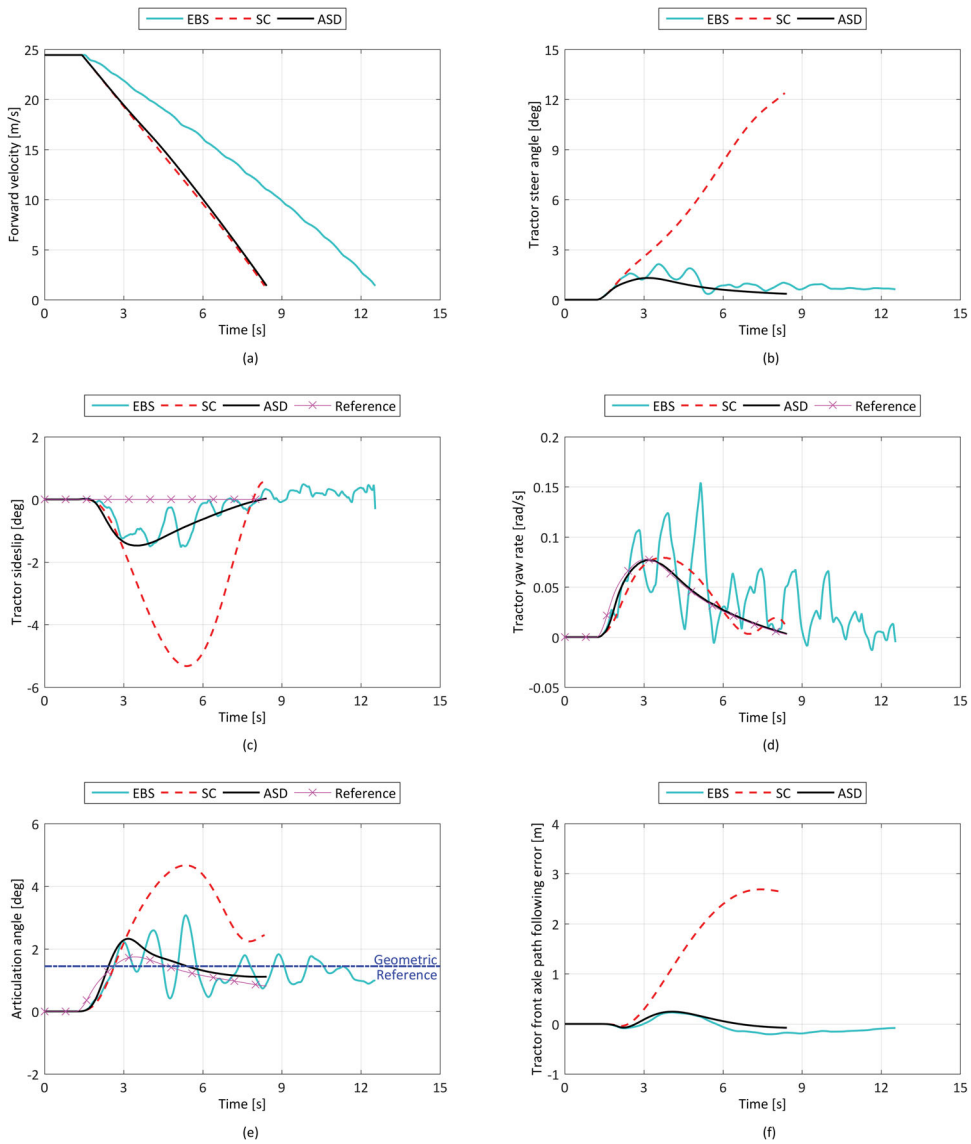
Figure 10. Three hundred metre radius J-turn simulation results with conventional EBS, SC and ASD braking: (a) forward vehicle speed; (b) tractor road–wheel steering angle; (c) tractor sideslip angle; (d) tractor yaw rate; (e) articulation angle and (f) tractor front axle path-following error.

performance achieved by ASD. The velocity trace almost exactly matches SC, with substantially greater deceleration than EBS. Tractor steering angle with SC rises to over 12 degrees as the driver model unsuccessfully tries to overcome the severe understeer, whereas with both EBS and ASD the peak steering angle is less than 1.5 degrees. The steering angle with ASD resembles a smoothed version of that with EBS, since the periodic tyre forces caused by anti-lock cycling led to significant oscillations of the vehicle state. Calculating the tyre sideslip angle at the front axle helps to demonstrate the severity of the understeer in the

SC case: over 13 degrees sideslip was observed, compared with less than 3 degrees for EBS and ASD.

In Figure 10(c), tractor sideslip angle for ASD resembles a smoothed version of EBS sideslip angle. It reaches a peak magnitude of less than 1.5 degrees, in comparison with over 5 degrees for SC. The yaw rate plot in Figure 10(d) also includes the reference yaw rate used by the ASD controller. The initial yaw acceleration with ASD is noticeably faster than with SC and yaw rate closely tracks the reference value, eliminating the previously observed understeer.

Figure 10(e) plots articulation angle, including both the ASD reference value and a 'geometric reference'. The geometric reference – an approximation of the vehicle's steady-state turning behaviour at very low speeds, included purely for comparison – was calculated by considering a single-track model of the vehicle following a constant 300 m radius curve, assuming the tractor front, tractor rear and trailer middle axles all travel with zero sideslip. After an initial transient peak, both the ASD articulation angle and the ASD reference return close to the geometric reference value of 1.4 degrees. The peak transient articulation angle with ASD is almost exactly half that of SC, suggesting that the risk of jack-knife is significantly reduced. Finally Figure 10(f) shows path-following error of the tractor front axle. The maximum error with ASD is less than 0.25 m, similar to EBS, in comparison to almost 3 m with SC.

Figure 11(a,b) plots the lateral and longitudinal forces (per single tyre) generated on the right-hand wheel of the trailer middle axle. Similar characteristics were observed when plotted for the vehicle's other axles. The large amplitude cycling of forces caused by conventional EBS can be seen. Peak longitudinal force is around the same magnitude with EBS as with SC, but SC maintains this level for the entire manoeuvre whereas EBS achieves it only periodically. Lateral tyre force is at times lower with EBS than with SC, but repeatedly peaks at considerably greater values. These intermittent peaks are sufficient to improve the vehicle's directional response.

Relatively small differences in longitudinal force exist between SC and ASD. The effect on lateral tyre force is much greater, with ASD achieving substantially higher peak force. This peak occurs earlier in the manoeuvre, responding far more quickly to the driver model's steering input. The lateral tyre force plot with ASD resembles a smoothed version of that with EBS.

Figure 11(c)–(e) compares the nominal and attenuated slip demands for the right-hand wheels of the tractor front, tractor rear and trailer middle axles during the manoeuvre with ASD, while Figure 11(f) plots the three slip attenuation factors. The nominal demands were attenuated by a maximum of 61%, 62% and 63% on the tractor front, tractor rear and trailer axles, respectively. Slip was first attenuated on the tractor front axle in order to enable the driver model to turn the vehicle, with slips on the tractor rear and trailer axles then subsequently being attenuated in order to prevent oversteer, excessive tractor sideslip or trailer swing-out.

4.2. Tuning for unknown conditions

The results above demonstrated the performance of the ASD controller when its three gains were optimised for the specific manoeuvre. To determine the sensitivity of the controller to these gains, a further 484 simulations were run for the same manoeuvre. K_β and K_r were
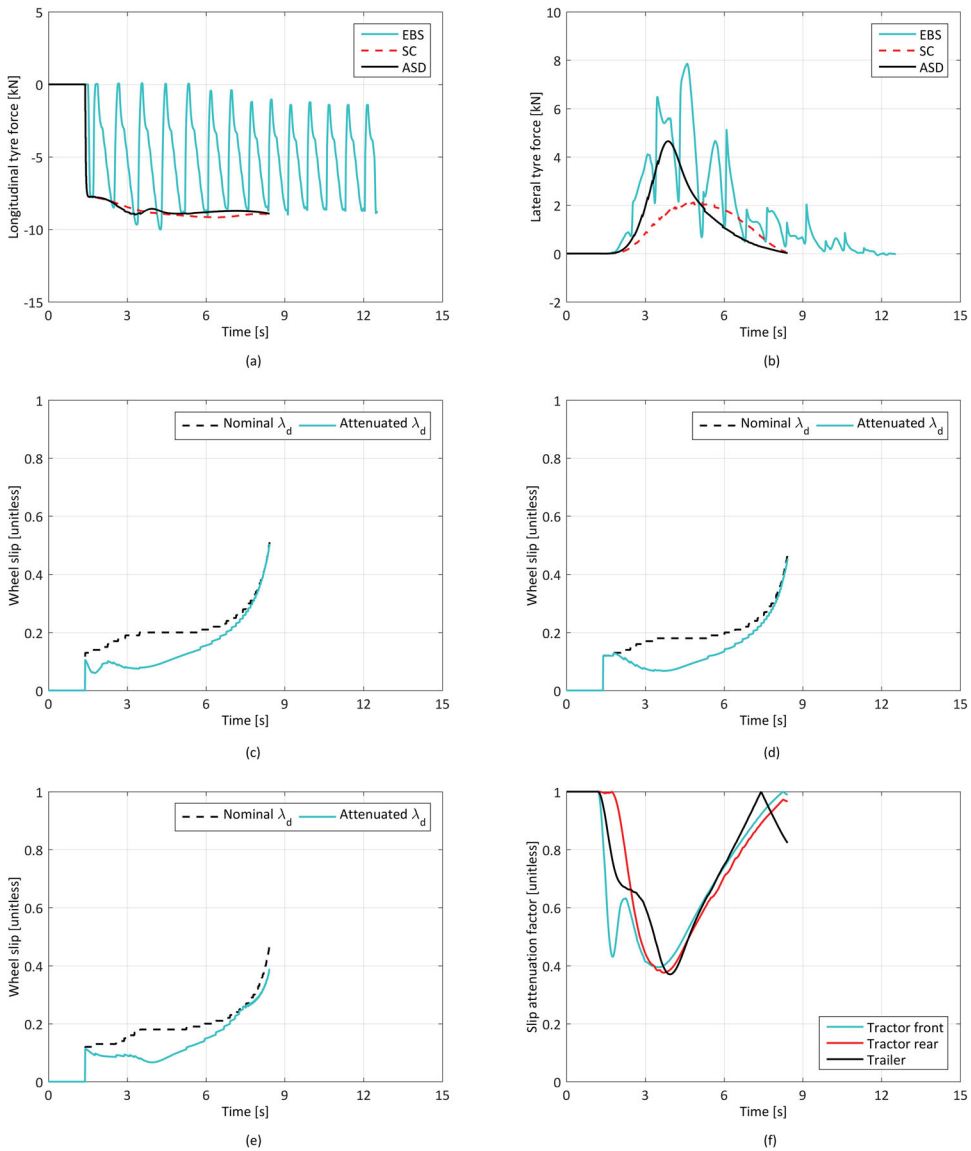
Figure 11. Three hundred metre radius J-turn simulation results with conventional EBS, SC and ASD braking: (a) longitudinal tyre force, trailer middle axle left wheel; (b) lateral tyre force, trailer middle axle left wheel; (c) slip demands, tractor front axle; (d) slip demands, tractor rear axle; (e) slip demands, trailer middle axle and (f) slip attenuation factors.

varied between 0 and 50 in increments of 5, while K_γ was set at 0, 10, 20 and 40 (with units of rad^{-1} for K_β and K_γ, and s/rad for K_r).

Figure 12 plots contours of two quantities as they vary with the three gains: (a) normalised mean deceleration (normalised by the mean deceleration of SC in the same manoeuvre, so that the best possible stopping performance gives a value of 1) and (b) maximum deviation of any point on the vehicle from the desired path. There are large areas of
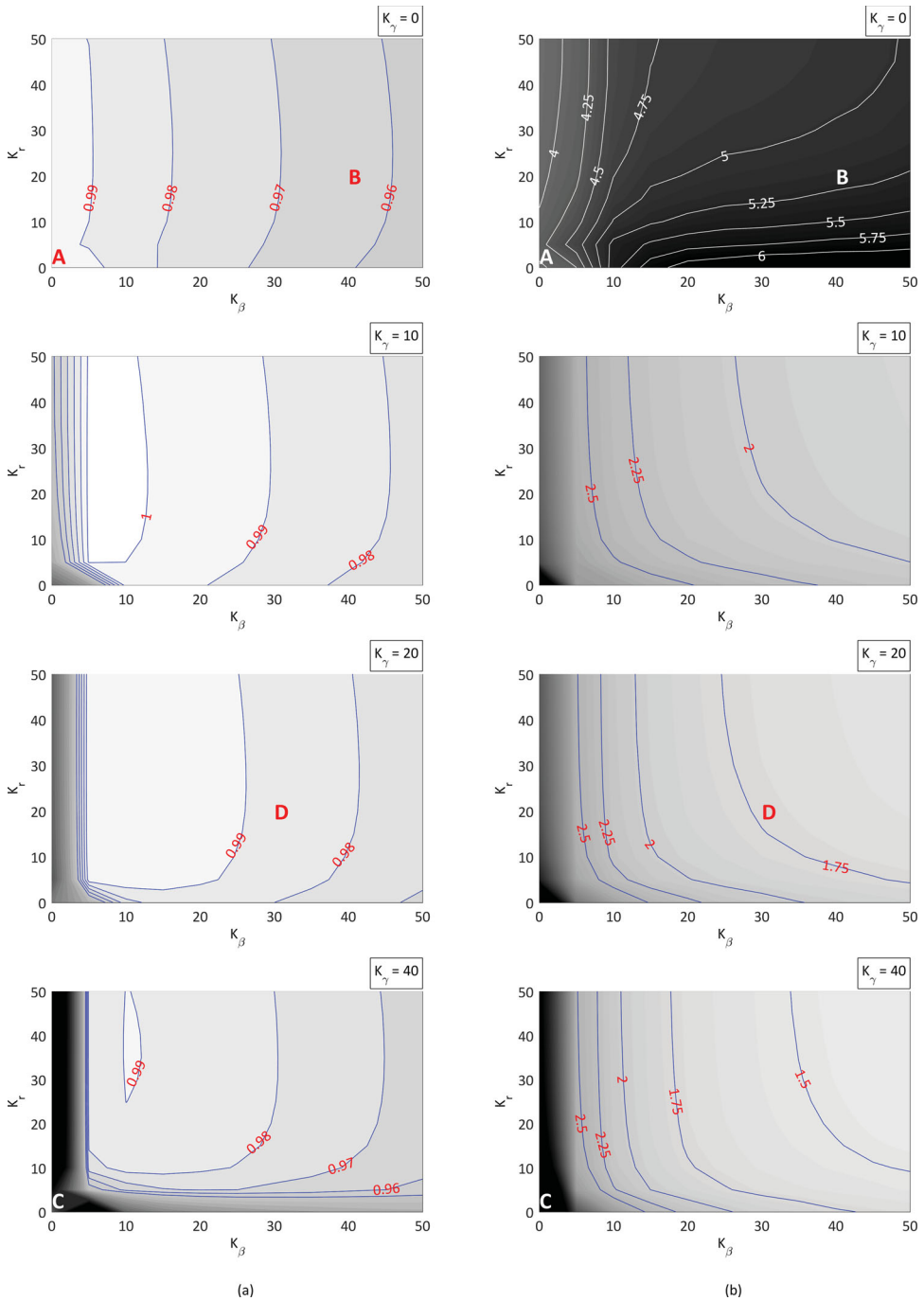
Figure 12. Overview of tuning space for ASD controller in 300 m radius J-turn with $\mu = 0.4$. Contours of: (a) normalised mean deceleration; (b) maximum deviation from path (m).

the tuning space in which normalised deceleration is close to 1. Also, provided the articulation angle gain K_γ is not too low, these large areas of near-optimal stopping performance have substantial overlap with those in which the maximum path deviation is small (e.g. less than 1.75 m in order to remain within a 3.5 m wide road lane).

Figure 13 shows animations of the manoeuvre for four different sets of gains, corresponding to the four points of interest marked A–D on the tuning space in Figure 12. These help to visualise the performance trade-offs between the three gains. The vehicle's behaviour at these points can be described as follows:

(a) $K_\beta = 0\,\text{rad}^{-1}$, $K_r = 0\,\text{s/rad}$ and $K_\gamma = 0\,\text{rad}^{-1}$ – ASD off or all gains too low: performance reverts to that of SC. Best possible stopping performance is achieved, but the vehicle understeers out of the road lane due to diminished lateral tyre forces at the tractor front axle.

(b) $K_\beta = 40\,\text{rad}^{-1}$, $K_r = 20\,\text{s/rad}$ and $K_\gamma = 0\,\text{rad}^{-1}$ – articulation angle gain K_γ too low: slip demands are attenuated on the tractor unit, allowing it to generate large enough lateral tyre forces to follow the desired path. However, trailer slip demands are not sufficiently attenuated. Therefore, the trailer swings out due to its diminished lateral tyre forces. Stopping distance is not significantly increased relative to case A.

(c) $K_\beta = 0\,\text{rad}^{-1}$, $K_r = 0\,\text{s/rad}$ and $K_\gamma = 40\,\text{rad}^{-1}$ – tractor gains K_β and K_r too low: as in case A the tractor initially understeers, because insufficient lateral forces are generated at the front axle. This causes the driver model to steer to a large angle in an attempt to compensate (an action that might also be expected from a human driver). This causes a large mismatch between the reference model and the actual vehicle state. With non-zero articulation angle gain, the large articulation angle error causes braking on the trailer to be attenuated substantially. This causes the trailer to 'push' the tractor unit around into jack-knife. Stopping distance also significantly increases due to the large attenuation of trailer braking.

(d) $K_\beta = 30\,\text{rad}^{-1}$, $K_r = 20\,\text{s/rad}$ and $K_\gamma = 20\,\text{rad}^{-1}$ – well selected gains: both tractor and trailer are able to remain within the road lane and follow the desired path, without any significant increase in stopping distance relative to case A.

Cases B and C might be considered even more dangerous than case A, in which ASD is turned off. However, from Figure 12, it is clear that these scenarios only occur in the far extremes of the tuning space when one or more of the gains are set very close to zero. The vast majority of the tuning space has qualitatively similar behaviour to case D. In these regions, performance of the ASD controller is remarkably insensitive to the gains used. This result is promising for real-world application of the controller, when the gains cannot be individually optimised for every possible operating scenario. It suggests that satisfactory ASD performance might be possible across a wide range of different manoeuvres without varying the controller gains.

Figure 14 plots mean deceleration and maximum path deviation for J-turn simulations of three different radii, each across a wide range of friction conditions. The initial speed was always 88 km/h. Conventional EBS, SC and two different versions of ASD are compared. The first version, 'optimised ASD', used gains which had been optimised specifically for each individual manoeuvre using the same optimisation procedure as in Section 4.1. The second version, 'invariant ASD', used the same set of gains across all scenarios. The optimal
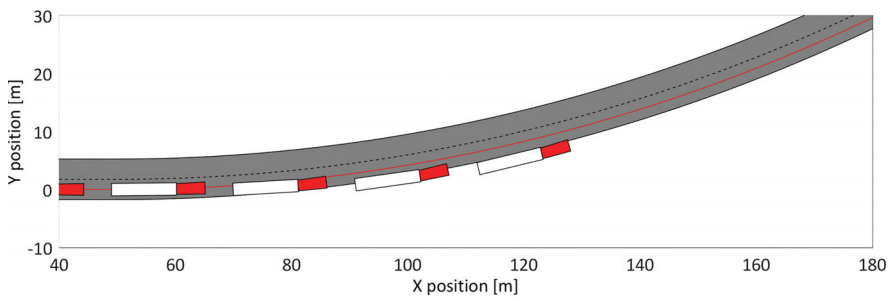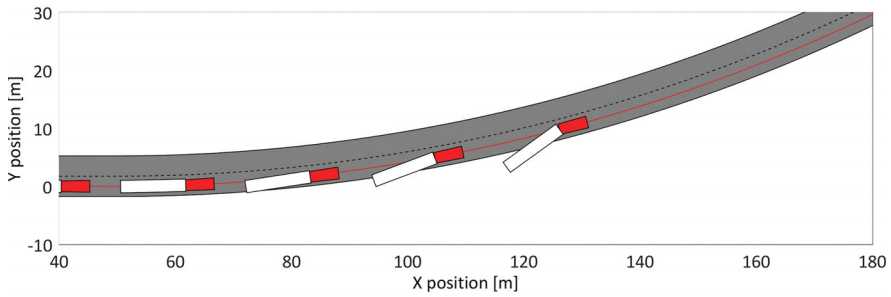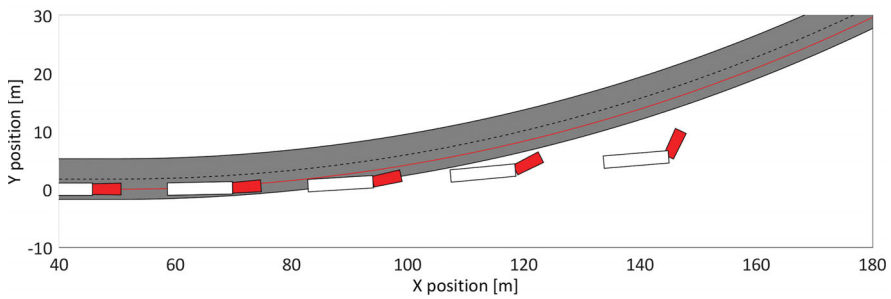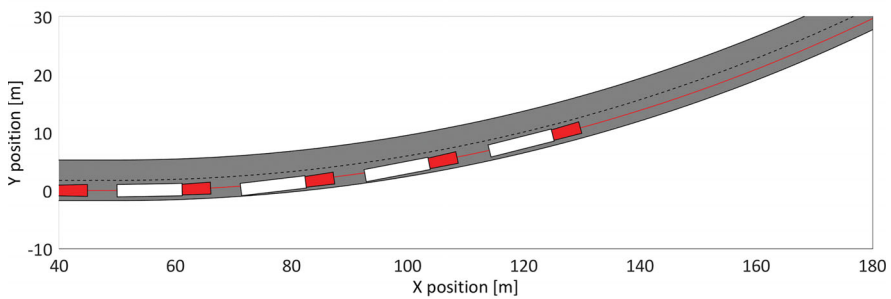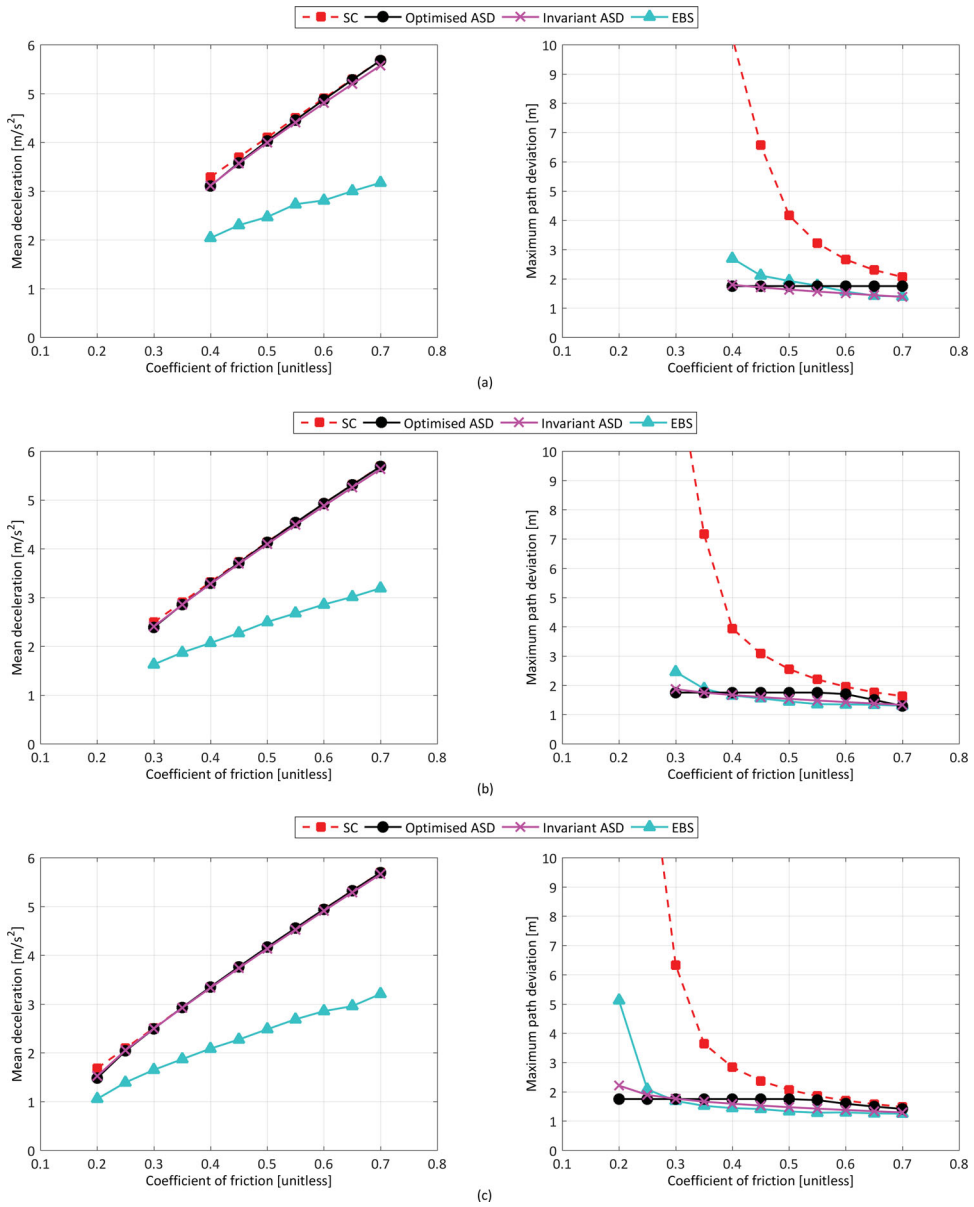
Figure 13. Animations of selected ASD controller tuning points from Figure 12: (a) A: $K_\beta = 0$, $K_r = 0$, $K_\gamma = 0$ – ASD off; (b) B: $K_\beta = 40$, $K_r = 20$, $K_\gamma = 0$ – trailer gain too low; (c) C: $K_\beta = 0$, $K_r = 0, K_\gamma = 40$ – trailer gain too large relative to tractor gains and (d) D: $K_\beta = 30$, $K_r = 20$, $K_\gamma = 20$ – well selected gains.

Figure 14. Performance of ASD with a single set of invariant gains in J-turn manoeuvres with a range of friction conditions. Comparison with conventional EBS, SC and ASD with gains optimised for each manoeuvre, with manoeuvre radii of: (a) 200 m; (b) 300 m and (c) 400 m.

gains from the 300 m radius J-turn with $\mu = 0.4$ ($K_\beta = 23.5\,\mathrm{rad}^{-1}$, $K_r = 34.6\,\mathrm{s/rad}$ and $K_\gamma = 30.8\,\mathrm{rad}^{-1}$) were used as the invariant gains, since in this manoeuvre both the optimised ASD and EBS only just remained within the road lane. Therefore, it would be acceptable for the invariant ASD to deviate from the lane in more severe manoeuvres than this (as would be expected), since the conventional EBS does the same.

In all of the scenarios, EBS showed significantly lower deceleration than all of the other braking strategies. At the highest simulated friction levels, little or no intervention was necessary from ASD in order to satisfy the lane-keeping constraint. Therefore, the difference in mean deceleration between optimised ASD and SC was negligible. The invariant ASD experienced a slight loss of mean deceleration in these conditions, though the maximum loss was just 1.8% compared to optimised ASD or SC. At these high friction levels, invariant ASD tended not only to remain in lane but to do so with room to spare, exhibiting path tracking comparable to or sometimes better than the conventional EBS.

At the lowest friction levels SC caused extremely large path deviations, therefore significant intervention was required by ASD in order to remain in the road lane and larger losses of mean deceleration occurred. The 400 m radius manoeuvre with $\mu = 0.2$ gave both the largest SC path deviation, at over 27 m, and the greatest loss of mean deceleration between invariant ASD and SC at 9.6%. Maximum path deviation with invariant ASD was a much reduced 2.2 m in this scenario, meaning a lane excursion of just 0.45 m. In any scenarios in which invariant ASD did not remain in the road lane, the lane excursion was less than with conventional EBS. By virtue of the strict lane-keeping constraint to which optimised ASD was bound, invariant ASD was able to slightly outperform optimised ASD in terms of deceleration in the lowest friction manoeuvres. In the 400 m radius J-turn with $\mu = 0.2$, for example, invariant ASD achieved 2.6% higher mean deceleration than optimised ASD.

To summarise:

(i) invariant ASD and optimised ASD produced similar performance levels across the full range of manoeuvres;
(ii) mean deceleration with invariant ASD tended to be marginally lower than with optimised ASD at the highest friction levels, but with a smaller maximum path deviation;
(iii) conversely, invariant ASD exhibited small lane deviations at the lowest friction levels in exchange for slightly improved mean deceleration over optimised ASD;
(iv) mean deceleration with ASD was always comparable to SC and substantially greater than with EBS, with the exception of one manoeuvre (400 m radius with $\mu = 0.2$) in which EBS caused a complete loss of directional control;
(v) maximum path deviation with invariant ASD was always less than with SC – substantially so at the lowest friction levels – and comparable to or less than with EBS;
(vi) in any case where invariant ASD experienced an exit from the road lane, the lane deviation was small and less than with EBS.

These results suggest that the ASD controller can indeed perform well across a wide range of operating conditions, even when using a single set of invariant gains.

4.3. Lane change manoeuvres

Figure 15 compares mean deceleration and maximum path deviation for single lane change manoeuvres of three different widths (3, 3.5 and 4 m wide, all with 61 m length, with an initial speed of 88 km/h), across a wide range of friction conditions. Only conventional EBS, SC and invariant ASD are plotted in this case, where invariant ASD used the same
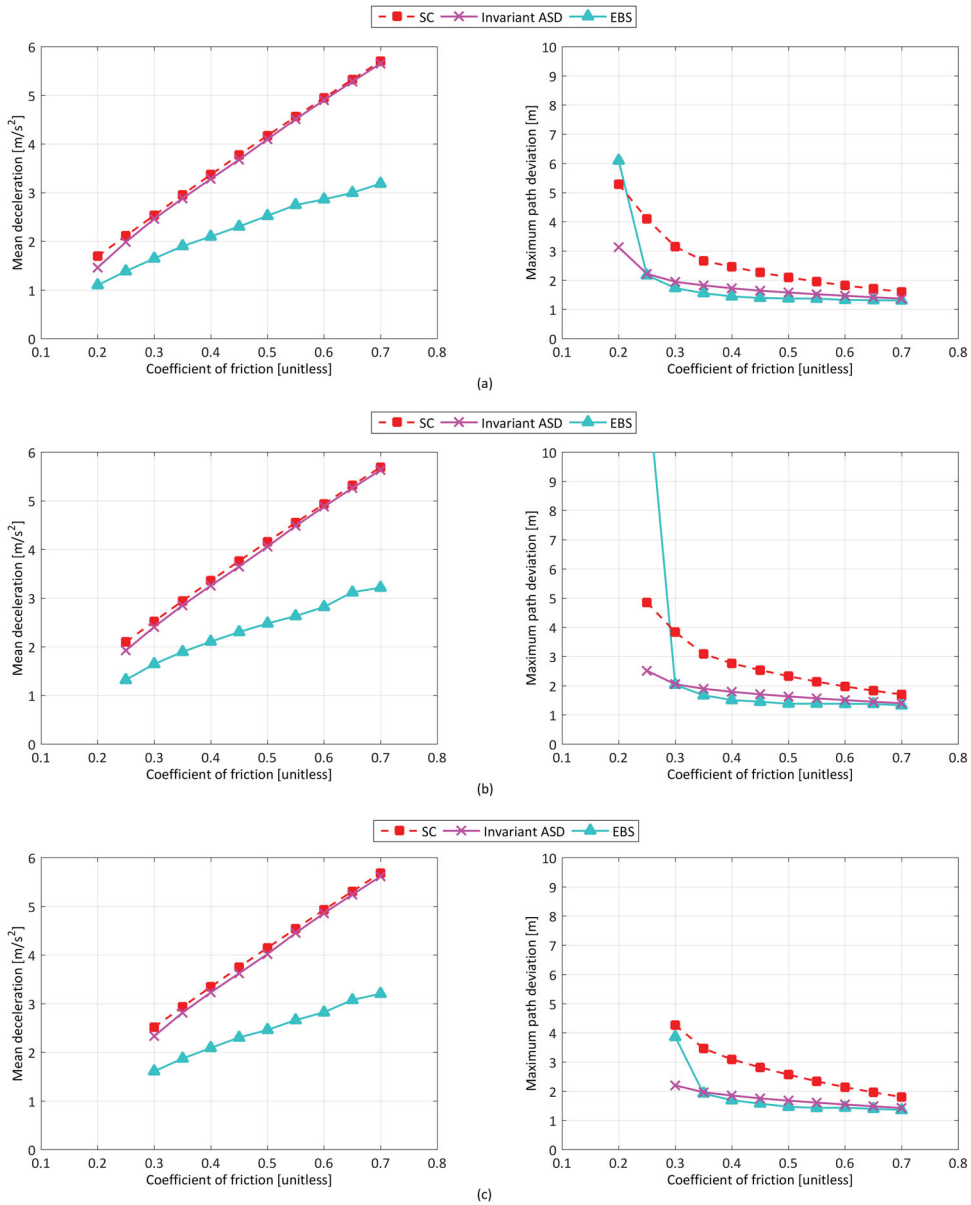
Figure 15. Performance of ASD with a single set of invariant gains in lane change manoeuvres with a range of friction conditions. Comparison with conventional EBS and SC with manoeuvre widths of: (a) 3 m; (b) 3.5 m and (c) 4 m.

gains as in the previous section. Similar to the J-turn manoeuvres, mean deceleration with ASD is always comparable to SC and much greater than with EBS, except at the lowest friction levels where EBS can cause a complete loss of directional control. ASD always reduces maximum path deviation compared to SC – substantially so at the lowest friction levels – and gives directional performance comparable to or better than EBS. In cases where ASD departs from the road lane, the deviation is small. In no scenario

does ASD exhibit a complete loss of directional control, unlike EBS at the lowest friction levels.

5. Conclusions and future work

Validated computer simulations of a tractor–semitrailer were used to compare combined emergency braking and cornering performance when using either a conventional HGV EBS or an idealised slip control braking system. The substantial stopping distance reduction possible with slip control was found to come at the expense of directional stability and controllability.

An 'ASD' controller was proposed to modify the slip control braking strategy. The controller compares observed vehicle states to a linear yaw-plane reference model, then attenuates the demanded wheel slips as necessary at each axle to restore directional control to the driver during emergency braking. Computer simulations suggested that the ASD controller maintained near-optimal stopping performance, while also matching conventional EBS in terms of directional performance. This could be achieved across a wide range of different manoeuvres and friction conditions using a single invariant set of controller gains.

A full-scale test vehicle is now being commissioned in order to experimentally validate the results of this paper. The test vehicle will be equipped with both a conventional EBS and the CVDC's prototype pneumatic slip control system. Combined emergency braking and cornering manoeuvres will be conducted on low friction surfaces to compare performance with conventional EBS and slip control with and without ASD. Results from these experiments will be published in due course.

Note

1. In modern 'electronic braking systems' for HGVs, the braking demand signal is sent to the brake controller (ECU) using an electronic signal, reducing the long delays caused by pneumatic signals in older anti-lock braking systems (ABS). However, the ECU still uses a conventional ABS algorithm to modulate the pneumatic pressure in the brake chambers, so as to prevent wheel lock-up. In this paper, 'EBS' refers to modern combined electronic/anti-lock braking systems of this description.

References

[1] Miller J, Cebon D. A high performance pneumatic braking system for heavy vehicles. Veh Syst Dyn. 2010;48(sup1):373–392.
[2] Hardy M, Cebon D. An investigation of anti-lock braking strategies for heavy goods vehicles. Proc IMechE, Part D: J Automob Eng. 1995;209(4):263–271.
[3] Kawabe T, Nakazawa M, Notsu I, et al. A sliding mode controller for wheel slip ratio control system. Veh Syst Dyn. 1997;27(5–6):393–408.
[4] Choi S, Cho D. Control of wheel slip ratio using sliding mode controller with pulse width modulation. Veh Syst Dyn. 1999;32(4–5):267–284.
[5] Wu M, Shih M. Simulated and experimental study of hydraulic anti-lock braking system using sliding-mode PWM control. Mechatronics. 2003;13(4):331–351.
[6] Akey M. Development of fuzzy logic ABS control for commercial trucks. SAE Technical Paper 952673, 1995.
[7] Wetherley B. Haldex electric brakes in action. Commercial Motor. November 2010:40.
[8] Seglo F. Brake-by-wire on heavy truck. Boras: HAVEit Final Event; 2011.
[9] Miller JI, Henderson LM, Cebon D. Designing and testing an advanced pneumatic braking system for heavy vehicles. Proc IMechE, Part C: J Mech Eng Sci. 2012;227(8):1715–1729.
[10] Miller J, Cebon D. Tyre curve estimation in slip-controlled braking. Proc IMechE, Part D: J Automob Eng. 2016;230(9). doi:10.1177/0954407015585934.
[11] Henderson L, Cebon D. Full-scale testing of a novel slip control braking system for heavy vehicles. Proc IMechE, Part D: J Automob Eng. Published Online Before Print, September 2015, doi:10.1177/0954407015604804.
[12] Henderson L, Cebon D. Straight-line braking comparison between EBS and a slip control braking system. Submitted to J Dyn Syst, Meas Control, 2016.
[13] Day AJ. Braking of road vehicles. Oxford: Butterworth-Heinemann; 2013.
[14] Dincmen E, Guvenc BA, Acarman T. Extremum-seeking control of ABS braking in road vehicles with lateral force improvement. IEEE Trans Control Syst Technol. 2014;22(1): 230–237.
[15] Kimbrough S. Stability enhancement and traction control of road vehicles. Int J Syst Sci. 1990;21(6):1105–1119.
[16] Kimbrough S. Rule based wheel slip assignment for vehicle stability enhancement. SAE Technical Paper 1999-01-0476, 1999.
[17] Kimbrough S, Elwell M, Chiu C. Braking controllers and steering controllers for combination vehicles. Int J Heavy Veh Syst. 1994;1(2):195–223.
[18] Fancher P. Generic data for representing truck tire characteristics in simulations of braking and braking-in-a-turn maneuvers. UMTRI 95-34, UMTRI, MI, USA, 1995.
[19] Morrison G. Combined emergency braking and cornering of articulated heavy vehicles. PhD Dissertation, Department of Engineering, University of Cambridge, Cambridge, UK, 2015.
[20] Miller J. Advanced braking systems for heavy vehicles. PhD Dissertation, Department of Engineering, University of Cambridge, Cambridge, UK, 2010.
[21] Kienhöfer F. Heavy vehicle wheel slip control. PhD Dissertation, Department of Engineering, University of Cambridge, Cambridge, UK, 2006.
[22] Henderson L. Improving emergency braking performance of heavy goods vehicles. PhD Dissertation, Department of Engineering, University of Cambridge, Cambridge, UK, 2013.

[23] Morrison G, Cebon D. Extremum seeking algorithms for the emergency braking of heavy goods vehicles. Submitted to Proc Instit Mech Eng, Part D: J Automob Eng., 2016.
[24] Morrison G, Cebon D. Sideslip estimation for articulated heavy vehicles in low friction conditions. IEEE Intelligent Vehicles Symposium. Seoul, Korea; 2015.
[25] Morrison G, Cebon D. Sideslip estimation for articulated heavy vehicles at the limits of adhesion. Veh Syst Dyn. 2016;54(11):1601–1628.
[26] HDEI/BCEI Working Group. FMS-standard description version 03; 2012. Available from: http://www.fms-standard.com/.
[27] Cheng C, Cebon D. Parameter and state estimation for articulated heavy vehicles. Veh Syst Dyn. 2010;49(1–2):399–418.
[28] Furukawa Y, Yuhara N, Sano S, et al. A review of four-wheel steering studies from the viewpoint of vehicle dynamics and control. Veh Syst Dyn. 1989;18(1–3):151–186.
[29] Nagai M, Shino M, Gao F. Study on integrated control of active front steer angle and direct yaw moment. JSAE Rev. 2002;23(3):309–315.
[30] Nagai M, Hirano Y, Yamanaka S. Integrated control of active rear wheel steering and direct Yaw moment control. Veh Syst Dyn. 1997;27(5–6):357–370.
[31] Nagai M, Hirano Y, Yamanaka S. Integrated robust control of active rear wheel steering and direct Yaw moment control. Veh Syst Dyn. 1998;29(sup1):416–421.

Appendix 1. State-space matrices of the ASD reference model.

$$A(u_1) = M^{-1}S,$$

$$B(u_1) = M^{-1}E,$$

$$M = \begin{bmatrix} (m_1 + m_2)u_1 & -m_2(l_{1c} + l_{2c}) & m_2 l_{2c} & 0 \\ -m_2(l_{1c} + l_{2c})u_1 & I_{1zz} + I_{2zz} + m_2(l_{1c} + l_{2c})^2 & -I_{2zz} - m_2 l_{2c}(l_{1c} + l_{2c}) & 0 \\ -m_2 l_{2c} u_1 & I_{2zz} + m_2 l_{2c}(l_{1c} + l_{2c}) & -I_{2zz} - m_2 l_{2c}^2 & 0 \\ 0 & 0 & 0 & 1 \end{bmatrix},$$

$$S = \frac{1}{u_1} \begin{bmatrix} -u_1(C_{\alpha,1f} + C_{\alpha,1r} + 3C_{\alpha,2}) \\ u_1(-l_{1f}C_{\alpha,1f} + l_{1r}C_{\alpha,1r} + 3(l_{1c} + l_{2c} + l_{2r})C_{\alpha,2}) \\ 3u_1(l_{2c} + l_{2r})C_{\alpha,2} \\ 0 \end{bmatrix}$$

$$\begin{array}{c} -l_{1f}C_{\alpha,1f} + l_{1r}C_{\alpha,1r} + 3(l_{1c} + l_{2c} + l_{2r})C_{\alpha,2} - (m_1 + m_2)u_1^2 \\ -l_{1f}^2 C_{\alpha,1f} - l_{1r}^2 C_{\alpha,1r} - (3(l_{1c} + l_{2c} + l_{2r})^2 + 2l_{2aa}^2)C_{\alpha,2} + (l_{1c} + l_{2c})m_2 u_1^2 \\ -(3(l_{2c} + l_{2r})(l_{1r} - l_{1cr} + l_{2c} + l_{2r}) + 2l_{2aa}^2)C_{\alpha,2} + m_2 l_{2c}u_1^2 \\ 0 \end{array}$$

$$\left. \begin{array}{cc} -3(l_{2c} + l_{2r})C_{\alpha,2} & -3u_1 C_{\alpha,2} \\ (3(l_{2c} + l_{2r})(l_{1c} + l_{2c} + l_{2r}) + 2l_{2aa}^2)C_{\alpha,2} & 3u_1(l_{1c} + l_{2c} + l_{2r})C_{\alpha,2} \\ (3(l_{2c} + l_{2r})^2 + 2l_{2aa}^2)C_{\alpha,2} & 3u_1(l_{2c} + l_{2r})C_{\alpha,2} \\ u_1 & 0 \end{array} \right],$$

$$E = \begin{bmatrix} C_{\alpha,1f} \\ l_{1f}C_{\alpha,1f} \\ 0 \\ 0 \end{bmatrix}.$$